

Molecular Characterization of DNA Double Strand Breaks with Tip-Enhanced Raman Scattering**

Ewelina Lipiec, Ryo Sekine, Jakub Bielecki, Wojciech M. Kwiatek, and Bayden R. Wood*

Abstract: DNA double strand breaks (DSBs) are deadly lesions that can lead to genetic defects and cell apoptosis. Techniques that directly detect DNA DSBs include scanning electron microscopy, atomic force microscopy (AFM), and fluorescence based approaches. While these techniques can be used to identify DSBs they provide no information on the molecular events occurring at the break. Tip-enhanced Raman scattering (TERS) can provide molecular information from DNA at the nanoscale and in combination with AFM provides a new way to visualize and characterize the molecular structure of DSBs. DSBs result from cleavage at the 3'- and 5'-bonds of deoxyribose upon exposure to UVC radiation based on the observation of P–O–H and methyl/methylene deformation modes enhanced in the TERS spectra. It is hypothesized that strand fragments are hydrogen-terminated at the lesion, indicating the action of free radicals during photon exposure.

DNA double strand breaks (DSBs) are deadly lesions that can lead to genetic defects and cell apoptosis^[1] There are several molecular pathways that can cause DSBs following ultraviolet C (UVC) exposure.^[2] Theoretically, 4.85 eV photons (the energy applied in this study) can damage DNA directly or indirectly, by the generation of delta electrons and free radicals, which react with the DNA molecule. The radiolysis products: free radicals ($\cdot\text{OH}$, $\cdot\text{H}$) can cause many kinds of DNA damage including single strand breaks (SSBs), DSBs, and cross-links.^[2] Recently it has been demonstrated

that even low-energy electrons of 0.1 to 2 eV can interact with double-stranded DNA and cause SSBs and DSBs.^[2–5] A study on isolated DNA in water, demonstrated that 99.5 % of the energy from ionizing radiation is absorbed directly by water and just 0.5 % by DNA.^[6]

Techniques that directly detect DNA DSBs include scanning electron microscopy,^[7] atomic force microscopy (AFM),^[8–10] and fluorescence-based approaches.^[11–15] While these techniques can be used to identify DSBs they provide no information on the molecular events occurring at the break. Tip-enhanced Raman scattering (TERS) can provide molecular information from DNA at the nanoscale^[16–18] and in combination with AFM provides a new way to visualize and characterize the molecular structure of DSBs. The primary use of AFM in this study is to identify potential sites of DSBs, which can then be targeted with TERS. TERS exploits the near-field enhancement generated by laser excitation of surface plasmons resulting in a strong electromagnetic field generated at the laser-irradiated apex of a metal or metalized scanning probe microscopy (SPM) tip.^[19–21] In this study, DNA dissolved in buffer was irradiated, then mixed with an untreated sample, and the DNA was then deposited onto a mica surface. By mixing irradiated and treated samples one could perform AFM and TERS measurements using the same tip and under the same conditions. AFM imaging was performed to locate target spots (control and broken DNA) based on the DNA molecule conformation determined by AFM topographical maps and AFM phase images. TERS spectra were collected from these target spots and the spectra (control and irradiated DNA) were analyzed with multivariate methods and compared with micro-Raman, SERS, and calculated spectra. The hypothesis is that a combination of AFM and TERS can be used to determine the chemical structure of individual DSB following UVC radiation exposure. It was found that DNA exposed to UVC resulted in three main types of chemical breaks the most important being cleavage at the 3'- and 5'- bonds of the deoxyribose unit resulting in terminal hydrogen bonding.


In this study pUC18 circular plasmid DNA was irradiated as a thin film in aqueous solution by a UVC lamp. The TERS methodology is described in sections S1 and S2 in the Supporting Information and includes an optical response image of the TERS tip (section S2) and a TERS image of DNA used to determine the absolute spatial resolution (section S3). A schematic diagram of the TERS upright configuration used to investigate irradiated DNA is shown in Figure 1 a. Mg^{2+} counterions are used to fix and orientate the DNA (Figure 1 b). To improve the enhancement and increase the percentage of functional TERS tips we coated one of the mica surfaces with a reflective silver coating and placed this

[*] E. Lipiec, Dr. J. Bielecki, Prof. Dr. W. M. Kwiatek
The Henryk Niewodniczanski Institute of Nuclear Physics
PAN, 31-342 Kraków (Poland)

E. Lipiec, Dr. R. Sekine, Assoc. Prof. B. R. Wood
Centre for Biospectroscopy, School of Chemistry
Monash University, 3800, Victoria (Australia)
E-mail: bayden.wood@monash.edu

Dr. R. Sekine
Centre for Environmental Risk Assessment and Remediation
University of South Australia
Mawson Lakes, 5095 SA Adelaide (Australia)

[**] This work was financially supported by an Australian Research Council future fellowship (grant number DP110104821). We would also like to acknowledge Prof. Małgorzata Lekka for advice on the preparation of the manuscript and Mr Finlay Shanks for instrumental support.

 Supporting information for this article, including methods (tips and samples preparation, AFM imaging, AFM imaging using TERS tips, TERS spectra collection), focusing of the laser on the tip, spatial resolution, spectral reproducibility for control and irradiated plasmid DNA, principal component analysis, micro-Raman spectroscopy, SERS and TERS, and a comparison of the TERS results with DFT calculations, is available on the WWW under <http://dx.doi.org/10.1002/anie.201307271>.

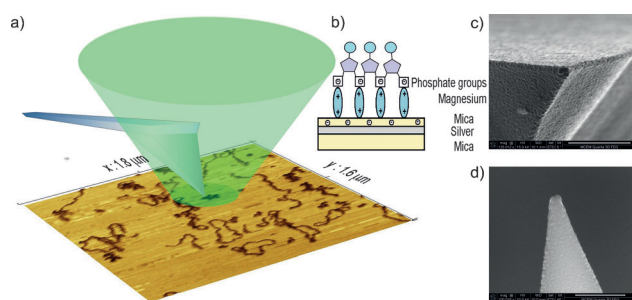


Figure 1. TERS configuration. a) AFM image of the pUC 18 DNA plasmid fixed onto a mica surface in the upright configuration showing the AFM tip and the direction of the green laser. b) Method of DNA fixation and substrate configuration. c, d) Scanning electron microscopic images of the silver-coated TERS tip. The scale bars are 500 nm.

underneath a second mica substrate (Figure 1b). This increases the amount of laser light in the tip area through reflection from the silver surface increasing the number of scattered photons interacting with the molecule and tip. The additional reflective surface leads to better enhancement and an increase in the percentage of TERS active tips (about 90%). This is because in the top-down configuration without a mirrored substrate the tip could cast a shadow on the sample at the measurement point and then the signal would not be enhanced. The mirrored surface illuminates more of the nanostructure at the tip apex, which is crucial in obtaining a higher percentage of active tips.^[22] Figure 1c and 1d shows scanning electron microscopic (SEM) images from different orientations of the nanodroplet of silver deposited on the AFM tip.

Figure 2 shows the AFM topography of control and irradiated samples. Untreated plasmid forms are dissolved in the solution and are supercoiled with some six to ten nodes observed.^[23] When the plasmid is damaged and providing there is at least one SSB it loses its supercoiled quaternary structure and goes into a relaxed state or a linear shape if there is a DSB.^[10–12, 22] The corresponding histograms show the averaged number of supercoiled, relaxed, and linear forms for control and irradiated DNA. For the actual TERS measurements, the control and irradiated solutions were mixed, enabling the collection of spectra from supercoiled control DNA and at the end points of linear DNA where the DSBs occur based on height and phase AFM images.

At the nanoscale the DNA is not homogenous, so each spectrum is recorded from a different set of base combinations (ca. 54 base pairs including the terminal groups are located in the near field of the tip; see section S3) and so variation is expected. The spatial resolution of our system (measured by mapping) was about 18.2 nm and the distance between two neighboring DNA base pairs (including one base pair) is 0.34 nm. The averaged number of base pairs located in the area of interest (in the near field of the tip) is calculated based on these approximations.

To assess the intrinsic variability associated with TERS measurements both the intra-sample and inter-sample variability were analyzed by both visual inspection and principal component analysis (PCA). Section S4 shows the variability

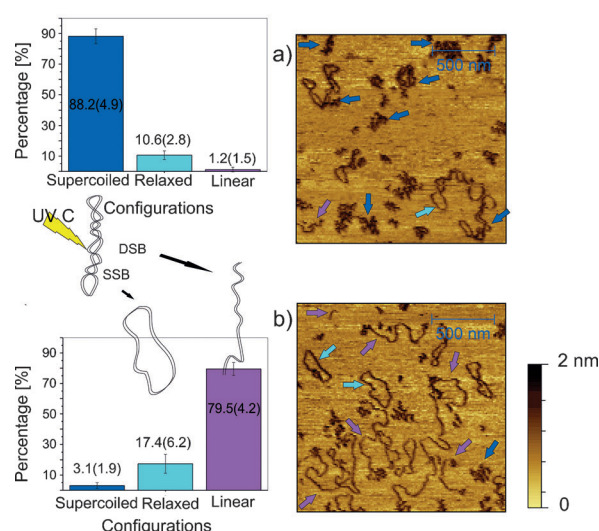


Figure 2. AFM topographies of plasmid DNA. a) Control plasmid DNA and b) pUC18 circular plasmid DNA exposed to 85 kJ m^{-2} UVC (256 nm) radiation. The histograms summarize the averaged number of supercoiled, relaxed, and linear plasmid forms corresponding to all control and irradiated samples. Three detectable plasmid forms were marked by arrows: supercoiled (blue), relaxed (cyan), and linear (pink).

observed from one tip for control and DSBs. TERS spectra from 350 different positions of control and DSBs in plasmid DNA were collected using seven different tips and analyzed with PCA. The results are presented in the section S5. By visualizing the data using a 3-dimensional PCA scores plot (PC1 vs. PC2 vs. PC3) it became apparent that different tips yield different spectral profiles although general clustering of the control and DSBs could be observed.

Figure 3a–c show schematics of the potential cleavage sites and terminal hydrogen-bonding sites based on detailed analysis of the TERS spectra. Figure 3 (right) shows three general types of representative TERS spectra designated type 1, 2, and 3 that were identified by a combination of PCA and visual inspection. Figure 3 (left) shows the three corresponding mechanisms that are hypothesized to lead to DSB formation based on the spectral interpretation. Broken bonds are marked with yellow and blue arrows. Type 1 spectra (Figure 3a) show strong bands corresponding to the CH_3 functional group. The schematic above the spectrum shows the position of the bond cleavage where the CH_3 group is bound. The appearance of CH_2/CH_3 (1368 cm^{-1}) scissoring modes along with the CH_2 (1439 cm^{-1}) deformation mode confirms that cleavage occurred at the 5'-bond position in a single DNA strand. Type 1 spectra do not exhibit the characteristic phosphodiester vibrations. This could be explained if the phosphodiester functional groups were removed upon the exposure to UVC radiation. If the absence of phosphodiester motions are indeed indicative of phosphate removal then this, suggests 3'-bond cleavage on the second DNA strand. Type 2 (Figure 3c) spectra, collected from regions of DSBs, show the phosphodiester vibrations and a strong signal from P–O–H in-plane bending mode at 1160 cm^{-1} , which is coupled to the P–OH stretching mode at

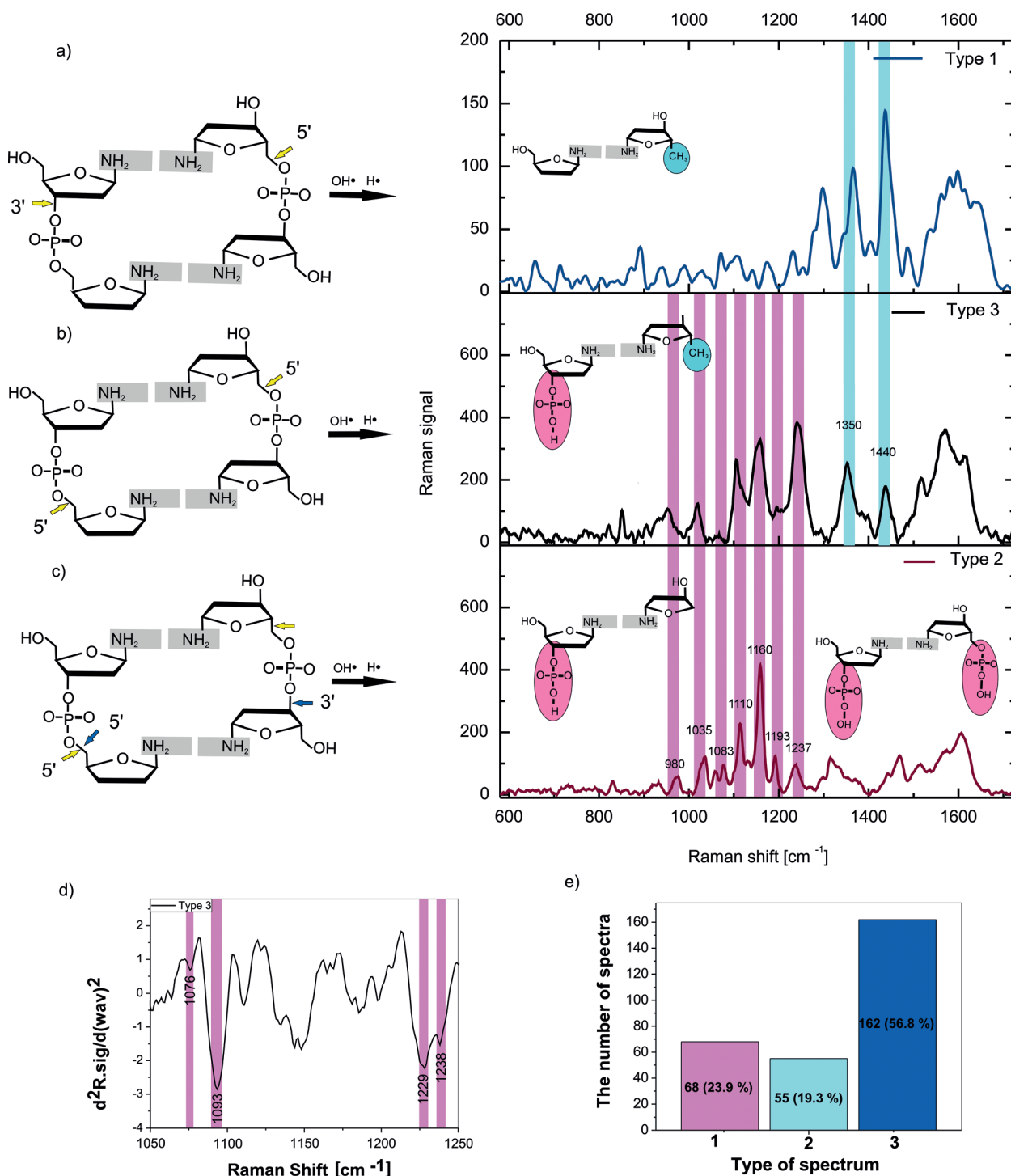


Figure 3. Potential cleavage sites and corresponding assigned TERS spectra. a) Type 1, b) type 3 (mixture of type 1 and type 2) and c) type 2 spectra. The blue highlight shows bands common to type 1 and type 3 spectra [1350 cm^{-1} $\delta(\text{CH}_2\text{CH}_3)$ out of plane, 1440 cm^{-1} $\delta(\text{CH}_2)$ in plane], whereas the pink shadow highlights bands common to type 2 and type 3 spectra [980 cm^{-1} $\nu(\text{C}=\text{O})$ ribose T, 1035 cm^{-1} $\nu(\text{C}=\text{O})$, 1083 cm^{-1} $\nu_{\text{sym}}(\text{O}-\text{P}-\text{O})$, 1110 cm^{-1} $\nu_{\text{sym}}(\text{O}-\text{P}-\text{C})$, 1160 cm^{-1} $\nu(\text{P}-\text{OH})$, 1193 cm^{-1} $\delta(\text{P}-\text{O}-\text{H})$ in plane, 1237 cm^{-1} $\nu_{\text{asym}}(\text{O}-\text{P}-\text{O})$]. The arrows indicate the potential cleavage sites that become hydrogen terminated. c) Second derivative of the type 3 spectrum zoomed in the spectral range of 1250 – 1050 cm^{-1} . d) The number of type 1, type 2, and type 3 spectra collected in this experiment.

1190 cm^{-1} [24,25] confirming that the phosphodiester fragment is hydrogen-terminated at the lesion site. The appearance of these bands indicates 3'-bond cleavage occurred in one strand and 5'-bond cleavage on the second strand (blue arrows). In

the present case, there also exists a second possible cleavage site (yellow arrows).

Close inspection of the asymmetric and symmetric phosphodiester bands (1240 – 1225 cm^{-1} and 1090 – 1070 cm^{-1})

of DNA reveals distinct shoulder features not observed in spectra recorded with the micro-Raman system. By applying a second derivative to the type 3 spectrum two sets of doublet bands are clearly resolved (Figure 3d). The appearance of these doublets is consistent with the phosphodiester groups being in slightly different molecular environments following the breakage and demonstrates the extremely high sensitivity that can be achieved with TERS. Type 3 spectra (Figure 3b) appear to be the sum of type 1 and type 2 spectra. Bands from the phosphodiester vibrations and the CH_3 group are observed, along with the bands at 1160 and 1190 cm^{-1} , indicating that radicals resulting from UVC irradiation preferentially attack O–C bonds. In Figure 3e a histogram showing the percentage of the three described types of TERS spectra is presented. The histogram shows that Type 3 spectra were collected more often than Type 1 or Type 2 spectra indicating that O–C ($5'$) cleavage is the most common form of cleavage. This result suggests that the O–C bond in the DNA backbone is the most sensitive to UVC radiation and its cleavage causes DSBs the majority of the time. The spectroscopic evidence for cleavage at the O–C band includes the identification of intense bands associated with the CH_2/CH_3 and P–O–H bending modes. To correlate the TERS measurements we compared the results with those obtained with surface-enhanced Raman (SERS) and conventional Raman spectroscopy. UVC-exposed DNA showed higher intensity bands in both SERS and micro-Raman compared to the controls. The SERS spectra resemble the TERS type 3 spectra showing enhanced phosphodiester and CH_2 deformation modes. These results are presented and explained in detail in section S6.

Additionally computations of Raman activity for control (undamaged) and damaged (type 3: $5'$ C–O cleavage) DNA structures have been carried out in the framework of hybrid QM/MM (quantum mechanics/molecular mechanics) method (ONIOM model). The technical details including a comparison of experimental and calculated spectra are described in section S7. The calculated spectra show good agreement for the band positions of the hydrogen terminated functional groups following $5'$ C–O bond cleavage including the P–O–H bending, P–OH stretching along with methyl/methylene deformation modes and the DNA phosphodiester modes.

We have shown that the combination of AFM-TERS provides a new way to visualize DNA and investigate the molecular structure of terminal groups at high spatial resolution and with extreme sensitivity. Moreover, we have demonstrated the potential of TERS to investigate the susceptibility of bonds to radiation damage and in particular have shown that O–C cleavage is the most likely form of DNA damage as this accounted for more than half of the cleavages detected.

Received: August 19, 2013

Published online: November 15, 2013

Keywords: atomic force microscopy · DNA damage · double strand breaks · tip-enhanced Raman scattering

- [1] R. Ugenskiene, J. Lekki, W. Polak, M. Prise, M. Folkard, O. Veselov, Z. Stachura, W. M. Kwiatek, M. Zazula, J. Stachura, *Nucl. Instrum. Methods Phys. Res. Sect. B* **2007**, 260, 159–163.
- [2] R. Barrios, P. Skurski, J. Simons, *J. Phys. Chem. B* **2002**, 106, 7991–7994.
- [3] J. Berdys, I. P. Anusiewicz, J. Simons, *J. Phys. Chem. A* **2004**, 108, 2999–3005.
- [4] I. P. Anusiewicz, J. Berdys, M. Sobczyk, P. Skurski, J. Simons, *J. Phys. Chem. A* **2004**, 108, 11381–11387.
- [5] J. Berdys, P. Skurski, J. Simons, *J. Phys. Chem. B* **2004**, 108, 5800–5805.
- [6] C. Sonntag, *Free-Radical-Induced DNA Damage and Its Repair: A Chemical Perspective*, Springer, Berlin, **2006**.
- [7] M. Brezeanu, F. Trager, F. Hubenthal, *J. Biol. Phys.* **2009**, 35, 163–174.
- [8] Y. Jiang, P. Marszalek, *Microscopy IV: Sci. Technol. Appl. Educ.* **2010**, 1, 450–459.
- [9] K. Psonka, S. Brons, M. Heiss, E. Gudowska-Nowak, G. Taucher-Scholz, *J. Phys. Condens. Matter* **2005**, 17, 1443–1446.
- [10] C. Ke, Y. Jiang, P. A. Mieczkowski, G. G. Muramoto, J. P. Chute, P. E. Marszalek, *Small* **2008**, 4, 288–294.
- [11] E. M. Filippova, D. C. Monteleone, J. G. Trunk, B. M. Sutherland, S. R. Quake, J. C. Sutherland, *Biophys. J.* **2003**, 84, 1281–1290.
- [12] N. Crosetto, A. Mitra, M. J. Silva, M. Bienko, N. Dojer, Q. Wang, *Nat. Methods* **2013**, 10, 361–365.
- [13] J. A. Harrigan, R. Belotserkovskaya, J. Coates, D. S. Dimitrova, S. E. Polo, C. R. Bradshaw, *J. Cell Biol.* **2011**, 193, 97–108.
- [14] J. Seo, S. C. Kim, H. S. Lee, J. K. Kim, H. J. Shon, N. L. Salleh, *Nucleic Acids Res.* **2012**, 40, 5965–5974.
- [15] R. K. Szilard, P. E. Jacques, L. Laramée, B. Cheng, S. Galicia, A. R. Bataille, *Nat. Struct. Mol. Biol.* **2010**, 17, 299–305.
- [16] K. F. Domke, D. Zhang, B. Pettinger, *J. Am. Chem. Soc.* **2007**, 129, 6708–6709.
- [17] R. Treffer, R. Bohme, T. Deckert-Gaudig, K. Lau, S. Tiede, X. Lin, *Biochem. Soc. Trans.* **2012**, 40, 609–614.
- [18] R. Treffer, X. Lin, E. Bailo, T. Deckert-Gaudig, V. Deckert, *Beilstein J. Nanotechnol.* **2011**, 2, 628–637.
- [19] E. M. van Schroyen Lantman, T. Deckert-Gaudig, A. J. G. Mank, V. Deckert, B. M. Weckhuysen, *Nat. Nanotechnol.* **2012**, 7, 583–586.
- [20] R. Stöckle, C. Fokas, V. Deckert, R. Zenobi, B. Sick, B. Hecht, U. P. Wild, *Appl. Phys. Lett.* **1999**, 75, 160–165.
- [21] R. Stöckle, Y. D. Suh, V. Deckert, R. Zenobi, *Chem. Phys. Lett.* **2000**, 318, 131–136.
- [22] W. Zhang, X. Cui, O. J. F. Martin, *J. Raman Spectrosc.* **2009**, 40, 1338–1342.
- [23] Y. Jiang, M. Rabbi, P. A. Mieczkowski, P. E. Marszalek, *J. Phys. Chem. B* **2010**, 114, 12162–12165.
- [24] A. C. Chapman, L. E. Thirlwell, *Spectrochim. Acta* **1964**, 20, 937–947.
- [25] M. E. Rudbeck, S. Kumar, M. A. Mroginski, S. O. Nilsson, M. R. Blomberg, A. Barth, *J. Phys. Chem. A* **2009**, 113, 2935–2942.